20144109

Modeling and Control of Radial Force due to Electromagnetic Force in IPMSMs

Masato Kanematsu[1)] **Takayuki Miyajima**[1)] **Hiroshi Fujimoto**[1)] **Yoichi Hori**[1)]
Toshio Enomoto[2)] **Masahiko Kondou**[2)] **Hiroshi Komiya**[2)] **Kantaro Yoshimoto**[2)] **Takayuki Miyakawa**[2)]

1) The University of Tokyo, Graduate School of Frontier Sciences
Transdisciplinary Sciences Bldg., 5-1-5, Kashiwanoha,Kashiwa, Chiba, 227-8561, Japan
(E-mail: kanematsu@hflab.k.u-tokyo.ac.jp, fujimoto@k.u-tokyo.ac.jp)
2) Nissan Motor Co., Ltd. 1-1, Morinosatoaoyama, Atsugi-shi, Kanagawa, 243-0123, Japan

Received on February 28th, 2014
Presented at the EVTeC on May 24th, 2014

ABSTRACT: In this paper, various methods to reduce noise and vibration of IPMSMs are introduced, especially focused on radial electromagnetic force fluctuation. Electrical 2nd and 6th order radial force is known to cause serious noise and vibration problem. Firstly the method to reduce radial force by structural designing is introduced. Secondly the modelling and control method for decreasing 2nd and 6th radial force vibration is shown. Finally, general overview is disscussed to realize advanced motor designing and control technology.

KEY WORDS: Electromagnetic force, Radial force control, Electric Vehicle, Noise and vibration

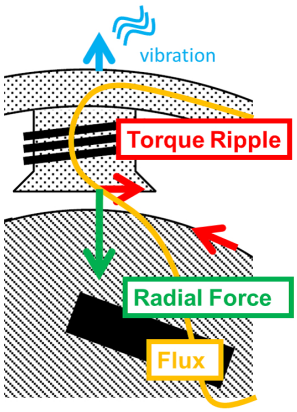

Fig. 1 The magnetic attractive force in IPMSMs

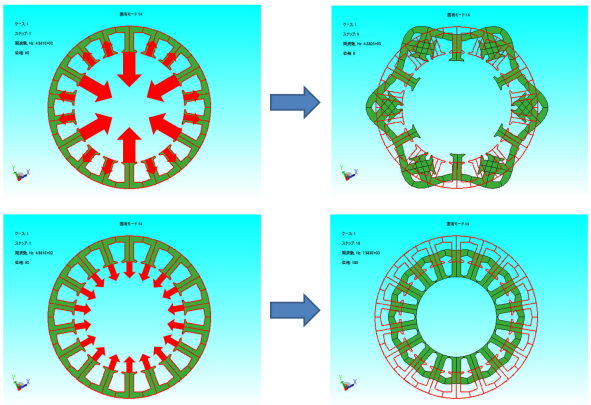

Fig. 2 typical radial force mode

1. Introduction

IPMSMs (Interior Permanent Magnet Synchronous Motors) are widely applied in many industrial applications. In these applications, IPMSMs face strong demands about the reduction of noise and vibration. In addition, the noise and vibration problems in the inside of cars remain to be one of the problems which should be improved. Furthermore, lower acoustic noise and vibration enhance the value of the product.

The magnetic attractive force which causes noise and vibration are produced by magnetic flux. Therefore it is important to grasp the flux distribution in IPMSMs. Fig. 1 shows the concept of magnetic attractive force. It can be seen that the magnetic attractive force has both the tangential and radial components in Fig. 1. Concentrated winding generally causes large fluctuation of tangential magnetic force which is called as torque ripple. Torque ripple triggers torsional resonant vibration and deteriorates control performance. On the other hand, the electromagnetic force fluctuation in radial direction is called as radial force and it induces elastic deformation when the frequency of radial force corresponds to natural frequency of the stator. Radial force is less acknowledged as a problem than torque ripple. However, in EV/HEV applications which are demanded very high performance, radial force comes to a head as the origin of noise and vibration. Fig. 2 shows typical radial force mode in IPMSMs.

In this paper, the cause of noise and vibration in radial direction due to electromagnetic force is classified into magnetostriction, rotor eccentricity, and rotating magnetic field. The methods to suppress each origin of noise and vibration by structural designing and control are overviewed. In these origins, We focus on the vibration caused by rotation magnetic field, and suppression methods by structural designing and current control proposed by our group are

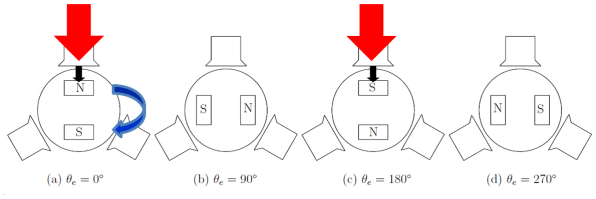

Fig. 3 Concept of 2nd radial froce

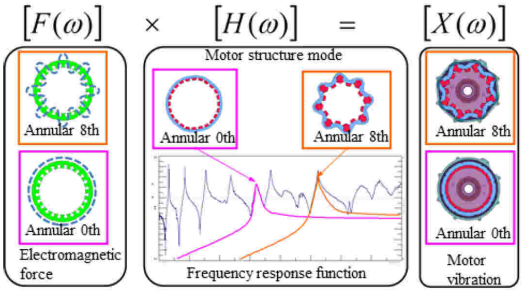

Fig. 4 The vibration mechanism(16P24S) [1] overviewed in this paper.

2. Fundamental concept of electromagnetic vibration

Vibration problem is generally formulated as :

$$[F(\omega)] \times [H(\omega)] = [X(\omega)] \tag{1}$$

where $[F(\omega)]$ is radial force, $[H(\omega)]$ is frequency response function and $[X(\omega)]$ is motor vibration. It is notable that frequency response function is constructed by various modes which are linearly independent set. Therefore vibration reduction should be performed to each modes.

It is known that in IPMSMs electrical 2nd and 6th radial force usually cause serious noise and vibration. 2nd radial force is caused by fundamental magnetic flux and the amplitude is very large. This leads to serious vibration although the corresponding frequency response function which mode is pole pair order annular mode is small. The concept of 2nd radial force is shown in Fig. 3. On the other hand, the amplitude of 6th radial force is small compared with 2nd radial force. However, the frequency response function which corresponds to 6th radial force is very large because 6th radial force excites spatially 0th annular mode.

Fig. 4 shows the vibration mechanism of 16P24S motor [1]. Fig. 4 also shows that in order to reduce motor vibrations there exist mainly two methods which are to improve the characteristics of frequency response function by structural designing and to reduce the fluctuation of radial force by current control. In (1) 3D map of the rotation speed, frequency, and vibration level is shown. As rotation speed increases, the frequency of the vibration also inreases.

3. Overview of previous study

3.1. Modelling of flux distribution

It has been studied for a long time the method to make the modelling of flux distribution in IPMSMs [2]. Z.Q.Zhu et al. generalize the modelling of flux distribution in previous researches (3)- (8). However, there are some faults in the studies that it is hard to apply this theory to actual application such as motor designing and current control designing. In (9) (10) and (11) this generalized modelling is extended to fractional order motor and modular winding motor [12] [13].

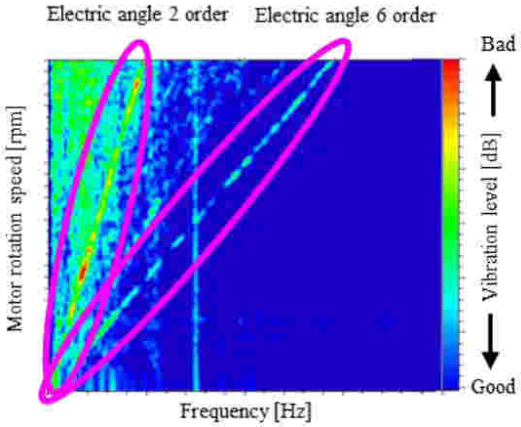

Fig. 5 3D map of vibration level [1]

3.2. Magnetostriction

The noise and vibration generated by magnetostriction is studied in (14). It is known that magnetostrictive force is hard to solve completely. Magnetostriction also deteriorates iron loss. To reduce the influence of magnetostriction, it is preferred to use magnetic steel sheets which have excellent property on magnetostriction. (15) also shows the influence of magnetostriction.

3.3. Rotor eccentricity

Rotor Eccentricity also contribute to the noise and vibration caused by electromagnetic force. When rotor eccentricity exists, unbalanced radial force is generated. This force attracts rotor to one side and leads to noise and vibration. There are many previous researches such as (16)- (21).

3.4. Causes of rotating magnetic field

Even if the two causes above don't exist, rotating magnetic field generates radial force ripple and it leads to noise and vibration. Radial force caused by rotating magnetic field is mainly electrical 2nd order. Considering the phase difference of U, V, and W-phase radial forces, it is known that 2nd order radial force has spatially Pth circular mode, in this sentence P denotes pole pairs. Until now, vibration reduction is mainly achieved by the structural designing based on Finite Element Analysis (FEA).

3.5. Reduction method By structural designing

In (22) peak amplitude of radial force is reduced by cutting the edge of teeth. Peak amplitude of radial force can be also decreased by making holes in the rotor [23] [25]. In (24) optimal stator design is studied with comparing some parameter of the motor topology. Skewing is well known to reduce cogging torque and torque ripple. Therefore it is

natural to apply skewing method for reducing radial force [26] [27] [28] [29]. In (1), to reduce 2nd order radial force, two structural designing methods to suppress motor vibration are proposed. One is to improve stator stiffness. Another method to suppress 2nd radial acceleration is to change pole slot combination. 2nd radial force excites mainly Pth spatial frequency. It means that the motor which has many pole pairs has low amplitude of transfer characteristic. The effect of changing pole slot combination is shown in (1) with experiments.

3.6. Reduction method by current control

On the other hand, few methods to suppress vibration using current control are proposed. (30) proposes radial force reduction with current control in condition of no-tooth effect. (31) and (32) propose harmonic radial force reduction method with harmonic current. These methods optimize current waveform through iterative calculation. (33) takes almost the same approach of (31) and lead the relationship between currents of U, V, and W-phase and radial force. Our group has already proposed curent control methods [34] [35], and they are overviewed in this paper.

4. Modelling and Control Technology to reduce 2nd radial vibration [34]

4.1. The Electromagnetic Forces of IPMSM

φ_m refers to the stator position angle between the center of a U-phase tooth and a point where maxwell stress is considered. Maxwell stress is expressed as

$$f_r(\varphi_m) = \frac{B_r^2(\varphi_m) - B_\theta^2(\varphi_m)}{2\mu_0}, \quad f_\theta(\varphi_m) = \frac{B_r(\varphi_m)B_\theta(\varphi_m)}{\mu_0} \tag{2}$$

where $B_r(\varphi_m)$ and $B_\theta(\varphi_m)$ are the radial and tangential maxwell stress on φ_m. In this paper, radial force $F_{rU,rV,rW}$ on the surface of U, V and W-phase teeth is evaluated.

$$F_{rU,rV,rW} = \int\int f_r(\varphi_m)\mathrm{d}S \tag{3}$$

where S is the surface area on a tooth facing on the air gap.

In this paper, radial force is calculated using approximate flux distribution. In this paper, JMAG (electromagnetic field analysis software with the FEA) produced by JSOL Corporation is applied to this analysis.

4.2. Approximate Model of Flux Distribution by Permanent Magnet

FEA result of flux distribution of permanent magnet is shown in Fig. 6. As shown in Fig. 6, The flux distribution is nearly flat on U-phase teeth, but unequal on V and W-phase teeth. Here, the flux distribution is approximated by rectangle. The magnetic flux passes through the area γS and no magnetic flux passes through the other area γS. where $\gamma(0 < \gamma \leq 1)$ is flux interlinkage area. It is expected that γ depends on rotor structure, but this relationship is

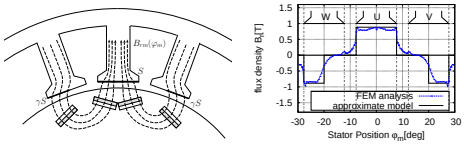

(a) magnetic flux lines (b) $B_{rm}(\varphi_m)$

Fig. 6 flux distribution $B_{rm}(\varphi_m)$ by permanent magnet

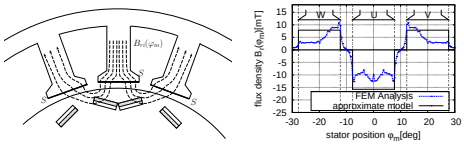

(a) magnetic flux lines (b) $B_{ri}(\varphi_m)$

Fig. 7 flux distribution $B_{ri}(\varphi_m)$ by d-axis current

inevident. In this paper, γ is determined from FEA, such that $\gamma = 1$ on U-phase and $\gamma = 0.5$ on V and W-phase.

The interlinkage flux $\psi_{mU,mV,mW}$ on a tooth surface is calculated as

$$\psi_{mU} = \psi, \quad \psi_{mV,mW} = -\frac{1}{2}\psi \tag{4}$$

where N is the number of turn/teeth, $\psi := \sqrt{\frac{2}{3}}\frac{\Psi_a}{PN}$. Here, coefficient $\sqrt{\frac{2}{3}}$ is the coeffficient to transform two-phase into three-phase.

The flux distribution of permanent magnet is approximated as $B_{rmj} = \frac{\psi_{mj}}{S_j}$, where B_{rmj} is flux interlinkage of j-phase teeth by permannet magnet, ψ_{mj} is interlinkage flux of j-phase, S_j is interlinkage flux area on j-phase teeth. Fig. 1 shows the approximate model of flux distribution.

4.3. Approximate Model of Flux Distribution by d-axis Current

Based on linear independency, B_{ri} is calculated by the diffenrence between B_r as $i_d = -1$[A] and by $B_{rm}(\varphi_m)$. Fig. 7 shows the flux distribution of $B_{ri}(\varphi_m)$. The flux distribution on U-phase tooth is nearly flat. On the other hand, the flux distribution on V and W-phase teeth concentrate in side of U-phase. In this paper, for the sake of simplicity, flux distribution on V and W-phase teeth is assumed to be flat.

$$\psi_{iU} = l_d i_d, \quad \psi_{iV,iW} = -\frac{1}{2} l_d i_d \tag{5}$$

where $\varphi_{iU,iV,iW}$ is flux on U, V and W-phase teeth by d-axis current. Here, l_d:=$\sqrt{\frac{2}{3}}\frac{L_d}{PN}$.

4.4. Radial force approximation using flux distribution

The flux distribution $B_r(\varphi_m)$ and maxwell stress $f_r(\varphi_m)$ on U-phase teeth are calculated as follows:

$$B_r(\varphi_m) = \left(\frac{\psi}{S} + \frac{l_d i_d}{S}\right) \tag{6}$$

By substituting (2) and (6) into (3), (8) is obtaind.

$$F_{rU} = \frac{B_r^2(\varphi_m)}{2\mu_0} \cdot S \tag{7}$$

$$= \frac{(\psi + l_d i_d)^2}{2\mu_0 S} \tag{8}$$

The flux distribution of PM is not flat on V and W-phase teeth. Therefore, approximate radial force is derived in two areas. In the area

$$B_r(\varphi_m) = \left(\frac{\psi}{2\gamma S} + \frac{l_d i_d}{2S}\right),\ B_r'(\varphi_m) = \frac{l_d i_d}{2S} \tag{9}$$

$$F_{rV}, F_{rW} = \frac{{B_r}^2(\varphi_m)}{2\mu_0} \cdot \gamma S + \frac{{B_r'}^2(\varphi_m)}{2\mu_0} \cdot (1-\gamma)S \tag{10}$$

$$= \frac{(\psi + l_d i_d)^2 + \frac{(1-\gamma)}{\gamma}\psi^2}{8\mu_0 S} \tag{11}$$

4.5. Current Reference Method to Suppress 2nd Order Radial Force

In this chapter, d-axis current reference is derived to suppress 2nd order radial force. $F_{rU}(\theta_e), F_{rV}(\theta_e)$, and $F_{rW}(\theta_e)$ refer to radial force of U, V and W-phase when rotor electrical angle is θ_e.

Generally, radial force is suppressed by reducing the difference between max. and min. radial force. When θ_e is $0, \pi$[rad], radial force on U-phase teeth is maximum and equals $F_{rU}(0)$, which is obtained in (8). Radial force reaches the a minimum value when θ_e is $\frac{1}{2}\pi$, $\frac{3}{2}\pi$[rad]. But, at this point, approximation model is not accurate enough. Therefore, radial force at $\theta_e = \frac{1}{3}\pi$[rad]is used instead of $\theta_e = \frac{1}{2}\pi$[rad]. If three-phase equilibrium is correct in IPMSM, $F_{rU}(\frac{2}{3}\pi)$ equals $F_{rV}(0)$. $F_{rV}(0)$ is approximated in (11). Moreover, by cyclic nature, $F_{rU}(\theta_e)$ has the equal values at electrical angle $\theta_e = \frac{1}{3}\pi, \frac{2}{3}\pi, \frac{4}{3}\pi, \frac{5}{3}\pi$[rad]. So, if following equation is true, it is predicted that 2nd radial force is suppressed largely.

$$F_{rU}(0) = F_{rU}\left(\frac{2}{3}\pi\right) \tag{12}$$

From (10), (13), (14), the d-axis current which achieves minimum 2nd order radial vibration is represented by

$$i_d = \left(-1 \pm \sqrt{\frac{1-\gamma}{3\gamma}}\right)\frac{\psi}{l_d} \tag{13}$$

By taking into consideration of $0 < \gamma \leq 1$, square root is real number. Here, plus sign in (13) is selected in order to use minimum current amplitude. Using Table. 1, d-axis current reference is calculated by

$$i_d = -29.1[\mathrm{A}] \tag{14}$$

4.6. Experiment

It is difficult to measure radial force directly. In this paper, radial acceleration outside the stator is evaluated in stead of radial force. The velocity is controlled by load motor. Drive motor controls current and radial acceleration on the stator of the drive motor is measured by accelerator.

In this paper, the negative d-axis current reference is limited within -20 A because of the motor rating. Experimental results with n = 1000, 2000 rpm are shown in Fig. 8(a), and 8(b) respectively. Here, the frequency of x-axis is normalized by electrical angle frequency. Fig. 8(a), and 8(b) shows d-axis current suppress 2nd order acceleration effectively, but deteriorate 6th order acceleration. 2nd order spectrums extracted in run-up experiment are shown in Fig. 8(c). 2nd order acceleration is suppressed at all rotation speeds.

5. Modelling and Control Technology to reduce 6th radial vibration [35]

5.1. The relationship between current, flux linkage and radial force

Flux passing through a U-phase tooth $\phi_u(t)$ is expressed with flux linkage in U-phase $\psi_u(t)$ as

$$\phi_u(t) = \frac{\psi_u(t)}{N}. \tag{15}$$

where, N is turn number per one phase, and all coils are connected as series. We assume the tangential flux distribution $B_\theta(t)$ is small, and all flux linkage is generated by the radial flux distribution $B_r(t)$. Radial force on a U-phase tooth $f_u(t)$ is calculated based on Maxwell stress. These assumptions are expressed as:

$$\phi_u(t) = \int B_r(t) dS, \quad f_u(t) = \int \frac{{B_r(t)}^2}{2\mu_0} dS. \tag{16}$$

where S is a tooth area facing air region. This paper has the assumption that flux is distributed equally over the tooth area S. With this assumption, (16) are rewritten as (17).

$$\phi_u(t) = B_r(t)S, \quad f_u(t) = \frac{B_r^2(t)}{2\mu_0} S \tag{17}$$

In this paper, we consider constant speed condition and radial force is regarded as a function for electrical angle θ. Substituting (15) into (17), radial force $f_u(t)$ is expressed as a function of $\psi_u(\theta)$.

$$f_u(\theta) = \frac{\psi_u^2(\theta)}{2\mu_0 S N^2} = A\psi_u^2(\theta), \quad A := \frac{1}{2\mu_0 S N^2} \tag{18}$$

(18) is used as the approximation of radial force in this paper.

5.2. Assumption on flux linkage

It is also assumed that flux linkage caused by permanent magnet $\psi_{um}(\theta)$ and flux linkage caused by current $\psi_{ui}(\theta)$ satisfy linear independency.

$$\psi_u(\theta) = \psi_{um}(\theta) + \psi_{ui}(\theta) \tag{19}$$

This paper considers 12 poles 18 slots IPMSM. The winding pattern is concentrated winding. To consider 6th radial force, $\psi_{um}(\theta)$ is defined as:

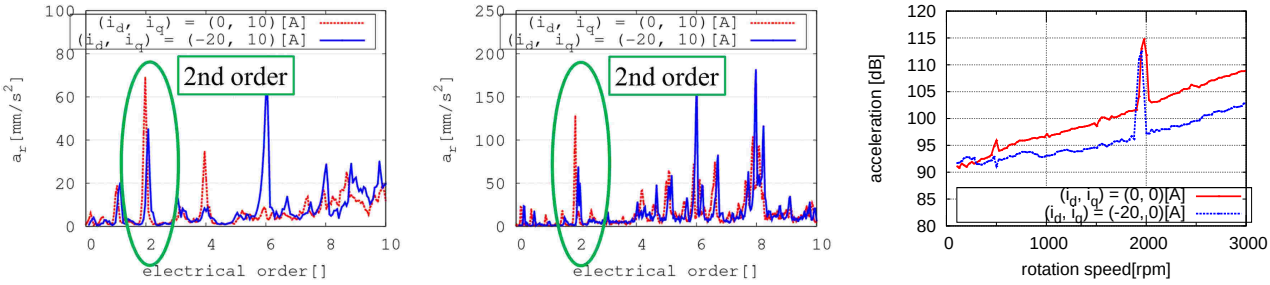

(a) 1000rpm (b) 2000rpm (c) comparison of 2nd order acceleration

Fig. 8 2nd radial force control(Experimental results)

Table 1 Parameters of IPMSM

turn number N	120
a pair of poles P	6
teeth area S [m^2]	4.13×10^{-4}
ψ_{m1}[mWb]	36.2
ψ_{m5}[mWb]	0.811
ψ_{m7}[mWb]	-0.114
L_d[mH]	0.866
L_q[mH]	1.31

$$\psi_{um}(\theta) = \psi_{1m}\cos\theta + \psi_{5m}\cos 5\theta + \psi_{7m}\cos 7\theta \quad (20)$$

5th and 7th flux linkage ψ_{5m} and ψ_{7m} have negative value when they have opposite phase against fundamental flux linkage. On ground of the symmetry, flux linkage on U-phase tooth is considered. The parameter of IPMSM is shown in Table 1. dq-axis current reference i_d, i_q is defined as :

$$i_d = I_{d0} + i_{d6}, \quad i_{d6} = I_{d6}\cos(6\theta - \theta_{d6}) \quad (21)$$

$$i_q = I_{q0} + i_{q6}, \quad i_{q6} = I_{q6}\cos(6\theta - \theta_{q6}). \quad (22)$$

5.3. The Influence of d-axis harmonic current

Flux linkage on U-phase caused by d-axis harmonic current $\psi_{ui(\theta)}$ is shown as:

$$\begin{bmatrix}\psi_{ui}(\theta)\\ \psi_{vi}(\theta)\\ \psi_{wi}(\theta)\end{bmatrix} = \boldsymbol{C}_{dq}^{uvw}\begin{bmatrix}L_dI_{d0} + L_dI_{d6}\cos(6\theta - \theta_{d6})\\ L_qI_{q0}\end{bmatrix}$$

$$= \sqrt{\frac{2}{3}}L_dI_{d0}\begin{bmatrix}\cos\theta\\ \cos(\theta - \frac{2}{3}\pi)\\ \cos(\theta - \frac{4}{3}\pi)\end{bmatrix} - \sqrt{\frac{2}{3}}L_qI_{q0}\begin{bmatrix}\sin\theta\\ \sin(\theta - \frac{2}{3}\pi)\\ \sin(\theta - \frac{4}{3}\pi)\end{bmatrix} \quad (23)$$

$$+\sqrt{\frac{1}{6}}L_dI_{d6}\begin{bmatrix}\cos(5\theta - \theta_{d6}) + \cos(7\theta - \theta_{d6})\\ \cos(5\theta - \theta_{d6} + \frac{2}{3}\pi) + \cos(7\theta - \theta_{d6} - \frac{2}{3}\pi)\\ \cos(5\theta - \theta_{d6} + \frac{4}{3}\pi) + \cos(7\theta - \theta_{d6} - \frac{4}{3}\pi)\end{bmatrix} \quad (24)$$

Substituting (24) (20) and (19) into (18) all radial force is calculated. It is presumable 6th radial force caused by d-axis harmonic currrent is considered as a function of drive condition I_{d0}, I_{q0} and d-axis harmonic current i_{d6}. Therefore, 6th radial force caused by d-axis harmonic current $f_{i_{d6}}(I_{d0}, I_{q0}, i_{d6})$ is extracted in (18) as:

$$f_{i_{d6}}(I_{d0}, I_{q0}, i_{d6}) = K_{dr}(I_{d0}, I_{q0})i_{d6} \quad (25)$$

$$K_{dr}(I_{d0}, I_{q0}) := \frac{A}{3}(\Psi_{1m} + L_dI_{d0})L_d \quad (26)$$

where, $\Psi_{1m} := \sqrt{\frac{3}{2}}\psi_{1m}$. In this paper, 2-phase/3-phase transform is absolute transformation. In Eq. (26), it is known that $f_{i_{d6}}$ are not affected by I_{q0}. To verify the accuracy of (26), FEA is performed on the condition that $I_{d6} = 1$ A and $\theta_{d6} = 0$ deg. The FEA result is shown in Fig.9(a) and 9(b). Although a lot of assumptions have been made to lead (26), we can see that 6th radial force model (26) differs very little from FEA result.

5.4. The Influence of q-axis Harmonic Current

In a similar way, flux linkage generated by current with d-axis harmonic current, $\psi_{ui}(\theta)$ is calculated as:

$$\begin{bmatrix}\psi_{ui}(\theta)\\ \psi_{vi}(\theta)\\ \psi_{wi}(\theta)\end{bmatrix} = \boldsymbol{C}_{dq}^{uvw}\begin{bmatrix}L_dI_{d0}\\ L_qI_{q0} + L_qI_{q6}\cos(6\theta - \theta_{q6})\end{bmatrix}$$

$$= \sqrt{\frac{2}{3}}L_dI_{d0}\begin{bmatrix}\cos\theta\\ \cos(\theta - \frac{2}{3}\pi)\\ \cos(\theta - \frac{4}{3}\pi)\end{bmatrix} - \sqrt{\frac{2}{3}}L_qI_{q0}\begin{bmatrix}\sin\theta\\ \sin(\theta - \frac{2}{3}\pi)\\ \sin(\theta - \frac{4}{3}\pi)\end{bmatrix} \quad (27)$$

$$+\sqrt{\frac{1}{6}}L_qI_{q6}\begin{bmatrix}\sin(5\theta - \theta_{q6}) - \sin(7\theta - \theta_{q6})\\ \sin(5\theta - \theta_{q6} + \frac{2}{3}\pi) - \sin(7\theta - \theta_{q6} - \frac{2}{3}\pi)\\ \sin(5\theta - \theta_{q6} + \frac{4}{3}\pi) - \sin(7\theta - \theta_{q6} - \frac{4}{3}\pi)\end{bmatrix} \quad (28)$$

Substituting (28) (20) and (19) into (18), the 6th radial force generated by q-axis harmonic current $f_{i_{q6}}(I_{d0}, I_{q0}, i_{q6})$ is extracted as:

$$f_{i_{q6}}(I_{d0}, I_{q0}, i_{q6}) = K_{qr}(I_{d0}, I_{q0})i_{q6}, \quad K_{qr}(I_{d0}, I_{q0}) := \frac{A}{3}L_q^2I_{q0} \quad (29)$$

Fig.9(c) shows the FEA results which are performed on the condition that $I_{q6} = 1$A, $\theta_{q6} = 0$A, and $I_{d0} = 0$A. Fig.9(c) shows that the Eq. (29) can predict 6th radial force caused by q-axis harmonic current well.

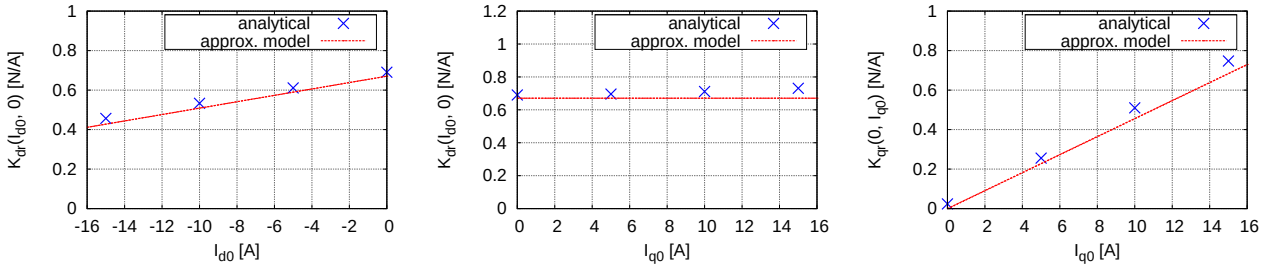

(a) $K_{dr}(I_{d0}, 0)$ (b) $K_{dr}(0, I_{q0})$ (c) $K_{qr}(0, I_{q0})$

Fig. 9 $K_{dr}(I_{d0}, I_{q0}), K_{qr}(I_{d0}, I_{q0})$ analysis result

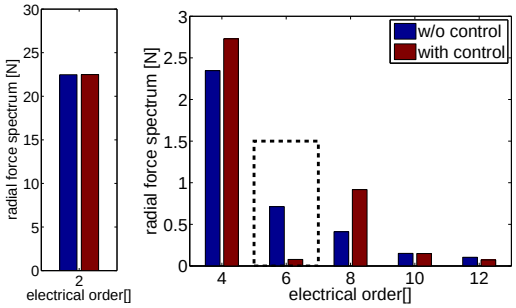

(a) 2 (b) 4-12th order

Fig. 10 6th radial force control(simulation result)

5.5. 6th radial force control

In this section, current reference to suppress 6th radial force is calculated based on 6th radial force modelling. All 6th radial force $f_{r6}(i_d, i_q)$ is expressed as :

$$f_{r6}(i_d, i_q) = f_{\text{base}}(I_{d0}, I_{q0}) + K_{dr}(I_{d0}, I_{q0}) i_{d6} + K_{qr}(I_{d0}, I_{q0}) i_{q6} \tag{30}$$

$$f_{\text{base}}(I_{d0}, I_{q0}) := F_{\text{base}} \cos(6\theta - \theta_{\text{base}}) \tag{31}$$

where, f_{base} is 6th radial force which is caused by harmonic inductance and harmonic magnet flux and it is calculated from FEA analysis on the condition that $i_{d6} = 0, i_{q6} = 0$. When d-axis harmonic current are used to suppress 6th radial force, optimal 6th harmonic d-axis current references $i_{d6:\text{opt}}$ to suppress 6th radial force are calculated with $F_{\text{base}}, \theta_{\text{base}}$ which is obtained from FEA analysis.

$$i_{d6:\text{opt}} = -\frac{F_{\text{base}}(I_{d0}, I_{q0})}{K_{dr}(I_{d0}, I_{q0})} \cos(6\theta - \theta_{\text{base}}) \tag{32}$$

Fig. 10 shows the simulation result of 6th radial force control with d-axis harmonic current. Current condition in Fig. 10 is $I_{d0} = 0, I_{q0} = 10$[A]. It is noticeable that 6th radial force is suppressed completely. 4th and 8th radial forces are also affected with d-axis harmonic current. However, the deterioration of 4th and 8th vibration caused by radial forces are small because the transfer characteristics of 4th and 8th radial force is small. This is remarked in following experimental result.

5.6. Experimental Results

In experiment, radial acceleration outside the stator is evaluated instead of radial force. The velocity is controlled at 800rpm by load motor. Current controller is designed as PI feedback controller and feedforward controller of Perfect Tracking Controller [36]. Optimal d-axis harmonic current reference is recalculated through experiment.

Experimental result is shown in Fig. 11. Large 6th radial vibration is observed in w/o control spectrum. Injecting optimal d-axis harmonic current, 6th radial vibration is suppressed largely.

6. Conclusion

In this paper, the origin of noise and vibration in IPMSMs are classified and the methods to reduce noise and vibration are overviewed. The quietness is one of the key technologies in future electric vehicles. Magnetostriction needs to be studied more and the reduction method of noise and vibration caused by magnetostriction is desired by the improvement of magnetic steel sheet and analysis technology. Uniformed modelling of radial force which shows structual designing and controller designing will be proposed in our future works.

References

(1) miyakawa, et. al: “Vibration mechanism of the motor for EV by analysis and An example of the vibration reduction countermeasures ”, JSAE Annual Congress in Spring, No.43-13(2013)(in Japanese)

(2) N.Boules: ”Prediction of No-Load Flux Density Distribution in Permanent Magnet Machines”, Industry Applications, IEEE Transactions on , vol.IA-21, no.3, pp.633-643, May 1985

(3) Z.Q.Zhu, D.Howe, E.Bolte, B.Ackermann: ”Instantaneous magnetic field distribution in brushless permanent magnet DC motors. I. Open-circuit field”, Magnetics, IEEE Transactions on , vol.29, no.1, pp.124-135, Jan 1993

(4) Z.Q.Zhu, D.Howe: ”Instantaneous magnetic field distribution in brushless permanent magnet DC motors. II. Armature-reaction field,” Magnetics, IEEE Transactions on , vol.29, no.1, pp.136-142, Jan 1993

(5) Z.Q.Zhu, D.Howe: ”Instantaneous magnetic field distribution in brushless permanent magnet DC motors. III. Effect of stator slotting”, Magnetics, IEEE Transactions on , vol.29, no.1, pp.143-151, Jan 1993

(6) Z.Q.Zhu, D.Howe: ”Instantaneous magnetic field distribution in permanent magnet brushless DC motors. IV. Magnetic field on load”, Magnetics, IEEE Transactions on, vol.29, no.1, pp.152-158, Jan 1993

(7) Y. S. Chen, Z. Q. Zhu, and D. Howe: “ Vibration of PM-brushlessmachines having a fractional number of slots per pole, ”IEEE Trans. Magn., vol. 42, no. 10, pp. 3395-3397, Oct. 2006.

(8) Z.Q.Zhu, L.J.Wu, Z.P.Xia: ”An Accurate Subdomain Model

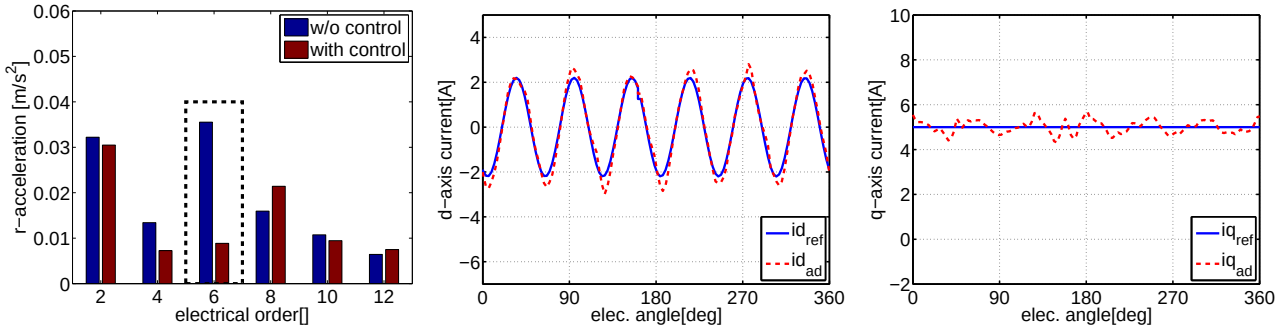

(a) r-acceleration (b) d-axis current (c) q-axis current

Fig. 11 6th radial force control (Experimental Results)

for Magnetic Field Computation in Slotted Surface-Mounted Permanent-Magnet Machines", Magnetics, IEEE Transactions on , Vol.46, No.4, pp.1100-1115, April 2010

(9) Zhu, Z.Q.; Xia, Z.P.; Wu, L.J.; Jewell, G.W. "Analytical Modeling and Finite-Element Computation of Radial Vibration Force in Fractional-Slot Permanent-Magnet Brushless Machines", Industry Applications, IEEE Transactions on, Vol.46, No.5, pp.1908-1918, , Sept.-Oct. 2010

(10) Jiabin Wang, Z.P.Xia, D.Howe, S.A.Long: "Vibration Characteristics of Modular Permanent Magnet Brushless AC Machines" Industry Applications Conference, 2006. 41st IAS Annual Meeting. Conference Record of the 2006 IEEE , Vol.3, No., pp.1501-1506, 8-12 Oct. 2006

(11) J.Wang, Z.P.Xia, S.A.Long, D.Howe: "Radial force density and vibration characteristics of modular permanent magnet brushless ac machine", Electric Power Applications, IEE Proceedings - , vol.153, no.6, pp.793-801, November 2006

(12) K. Atallah, J. Wang, and D. Howe: "Torque ripple minimization in modular permanent magnet brushless machines", IEEE Trans. Ind. Appl., vol.36, no.6, pp.1689-1695, 2003

(13) Jiabin Wang, Zhen Ping Xia, D.Howe: "Three-phase modular permanent magnet brushless Machine for torque boosting on a downsized ICE vehicle", Vehicular Technology, IEEE Transactions on , vol.54, no.3, pp.809-816, May 2005

(14) O.A.Mohammed, T.Calvert, R.McConnell : "Coupled magnetoelastic finite element formulation including anisotropic reluctivity tensor and magnetostriction effects for machinery applications", IEEE Trans.Magnetics, vol.37, no.5, pp.3388-3392(2001)

(15) F.Ishibashi,S.Noda,S.Yanase,T.Sasaki: "Magnetostriction and Motor Vibration", IEEJ Trans. A, Vol.123, No.6, pp.569-573, 2003(in Japanese)

(16) D.G.Dorrell, M.Popescu, D.M.Ionel: "Unbalanced Magnetic Pull Due to Asymmetry and Low-Level Static Rotor Eccentricity in Fractional-Slot Brushless Permanent-Magnet Motors With Surface-Magnet and Consequent-Pole Rotors", IEEE Trans. Magn., Vol.46, No.7, pp.2675-2685, July 2010

(17) U.Kim, D.K.Lieu: "Effects of magnetically induced vibration force in brushless permanent-magnet motors", IEEE Trans. Magn, vol.41, no.6, pp.2164-2172, June 2005

(18) A.Burakov, A.Arkkio: "Comparison of the Unbalanced Magnetic Pull Mitigation by the Parallel Paths in the Stator and Rotor Windings", IEEE Trans. Magn., Vol.43, No.12, pp.4083-4088, Dec. 2007

(19) J.T.Li, Z.J.Liu, L.H.A.Nay: "Effect of Radial Magnetic Forces in Permanent Magnet Motors With Rotor Eccentricity", IEEE Trans. Magn., vol.43, no.6, pp.2525-2527, June 2007

(20) Z.Q.Zhu, D.Ishak, D.Howe, C.Jintao: "Unbalanced Magnetic Forces in Permanent-Magnet Brushless Machines With Diametrically Asymmetric Phase Windings", IEEE Trans. Ind. Appl., vol.43, no.6, pp.1544-1553, 2007

(21) Z.Q.Zhu, L.J.Wu, M.L.M.Jamil: "Influence of pole and slot number combinations on cogging torque in permanent magnet machines with static and rotating eccentricities", IEEE the 2013 Energy Conversion Congress and Exposition (ECCE), pp.2834-2841, 15-19 Sept. 2013

(22) Y.Asano, Y.Honda, Y.Takeda, and S.Morimoto: "Reduction of Vibration on Concentrated Winding Permanent Magnet Synchronous Motors with Considering Radial Stress", IEEJapan Trans. D, Vol.121-D, No.11, pp.1185-1191, 2001(in Japanese).

(23) T.Kobayashi, Y.Takeda, M.Sanada, and S.Morimoto: "Vibration Reduction of IPMSM with Concentrated Winding by Making Holes", IEEJapan Trans. D, Vol. 124-D, No.2, pp. 202-207, 2004(in Japanese).

(24) Sang-Ho Lee, Jung-Pyo Hong, Sang-Moon Hwang, Woo-Taik Lee, Ji-Young Lee, Young-Kyoun Kim: "Optimal Design for Noise Reduction in Interior Permanent-Magnet Motor", IEEE Trans. Ind. Appl., vol.45, no.6, pp.1954-1960, Nov.-dec. 2009

(25) Jin Hur, Jin-Wook Reu, Byeong-Woo Kim, Gyu-Hong Kang: "Vibration Reduction of IPM-Type BLDC Motor Using Negative Third Harmonic Elimination Method of Air-Gap Flux Density", IEEE Trans. Ind. Appl., vol.47, no.3, pp.1300-1309, 2011

(26) D. C. Hanselman: "Effect of skew, pole count and slot count on brushless motor radial force, cogging torque and back EMF", Inst. Elect. Eng. Proc. mdash,Elect. Power Appl., Vol.144, No.5, pp.325-330, 1997

(27) Jae-Woo Jung; Do-Jin Kim; Jung-Pyo Hong; Geun-Ho Lee; Seong-Min Jeon: "Experimental Verification and Effects of Step Skewed Rotor Type IPMSM on Vibration and Noise", IEEE Trans. Magn., vol.47, no.10, pp.3661-3664, 2011

(28) A. Cassat, C. Espanet, R. Coleman, L. Burdet, E. Leleu,D. Torregrossa, J. M' Boua, A. Miraoui: "A Practical Solution to Mitigate Vibrations in Industrial PM Motors Having Concentric Windings", IEEE Trans. Ind. Appl., vol.48, no.5, pp.1526-1538, 2012

(29) TAKAHATA Ryoichi,WAKUI Shinichi,MIYATA Kenji,NOMA Keiji,SENOO Masaharu "Study on Reduction in Vibrations of Concentrated Winding Permanent Magnet Synchronous Motor by Skew Effects of Rotor", IEEJapan Trans. D, Vo.132, No.2, pp.278-287, 2012(in Japanese)

(30) G.Jiao, C.D.Rahn: "Field weakening for radial force reduction in brushless permanent-magnet DC motors, "IEEE Trans. Magn., vol. 40, no.5, pp. 3286-3292, Sep. 2004.

(31) W. Zhu, B. Fahimi, and S. Pekarek, " A field reconstruction method for optimal excitation of surface mounted permanent magnet synchronous machines, "IEEE Trans. Energy Convers., vol. 21, no. 2, pp. 303-313, Jun. 2006.

(32) D. Torregrossa, F. Peyraut, B. Fahimi, J. M 'Boua, and A. Miraoui, " Multiphysics finite-element modeling for vibration and acoustic analysis of permanent magnet synchronous machine "IEEE Trans. Energy Convers., vol. 26, no. 2, pp. 490-500, Jun. 2011.

(33) H.Yashiro, H.Takada: "Reduction of a Radial Electromagnetic Oscillating Force of an Electrical Motor by Superposing a High Order Current", the Japan Society of Mechanical Engineers Trans. C, Vol.72, No.715, pp.723-728, 2006(in Japanese)

(34) M.Kanematsu, T.Miyajima, H.Fujimoto, Y.Hori, T.Enomoto, M.Kondou, H.Komiya, K.Yoshimoto, T.Miyakawa: "Suppression Control of Radial Force Vibration due to Fundamental Permanent-Magnet Flux in IPMSM", IEEE Energy Conversion Congress and Exposition(ECCE), pp.2812-2816 (2013)

(35) M.Kanematsu, T.Miyajima, H.Fujimoto, Y.Hori, T.Enomoto, M.Kondou, H.Komiya, K.Yoshimoto, T.Miyakawa: "Proposal of 6th Radial Force Control Based on Flux Linkage – Verification on Load Condition –", The 2014 IEEE International Power Electronics Conference-ECCE ASIA-(IPEC), 2014

(36) K.Nakamura, H.Fujimoto, M.Fujitsuna: "Torque ripple suppression control for PM motor with current control based on PTC", Power Electronics Conference (IPEC), 2010 International , pp.1077-1082, June 2010